Catalysis Today 147 (2009) 260–269

Contents lists available at ScienceDirect

Catalysis Today

journal homepage: www.elsevier.com/locate/cattod

Combined *in situ* EXAFS and electrochemical investigation of the oxygen reduction reaction on unmodified and Se-modified Ru/C

Konstantin N. Loponov [a,1], Vladimir V. Kriventsov [a], Kyatanahalli S. Nagabhushana [b,2], Helmut Boennemann [b], Dimitrii I. Kochubey [a], Elena R. Savinova [c,*]

[a] Boreskov Institute of Catalysis, Russian Academy of Sciences, Pr. Akademika Lavrentieva 5, 630090 Novosibirsk, Russia
[b] Max-Planck-Institut für Kohlenforschung, Kaiser-Wilhelm-Platz-1, D 45470, Mülheim an der Ruhr, Germany
[c] l'Ecole Européenne Chimie Polymères Matériaux, Université de Strasbourg, UMR 7515 du CNRS-UdS-ECPM, 25, rue Becquerel, F-67087 Strasbourg, France

ARTICLE INFO

Article history:
Available online 23 February 2009

Keywords:
Electrochemical oxygen reduction reaction
Reaction kinetics and mechanism
Ru catalysts
Se-modification
X-ray absorption spectroscopy (XAS)
Rotating disc electrode
EXAFS

ABSTRACT

In this work we study the kinetics of the oxygen reduction reaction on carbon-supported Ru nanoparticles modified with various amounts of Se. Rotating disk electrode is used to determine kinetic currents for the ORR in 0.1 M H_2SO_4 at 298 K and O_2 partial pressures from 1 to 0.01 atm. The dependence of the ORR activity on Se/Ru ratio shows volcano-type behavior with ca. 10 fold increase of the mass activity at $0.1 < Se/Ru < 0.3$. The reaction order in O_2 is close to 1 in the interval of overpotentials from 0.4 to 0.7 V, and is independent of the presence of Se. Regardless the amount of Se, the Tafel slope demonstrates continuous increase from ca. 70 mV/dec at 0.4 V to ca. 140 mV/dec at 0.6 V overpotential. *In situ* EXAFS spectra are measured at Ru K-edge (in the transmission mode) and Se K-edge (in the fluorescence mode) in argon and oxygen saturated 0.1 M H_2SO_4 solutions in the interval of electrode potentials from 0.050 to 0.750 V RHE. The data are used to explore the surface state changes of Ru and Ru_xSe_y particles and clarify the promoting role of Se during the ORR.

1. Introduction

The Oxygen Reduction reaction (ORR) is one of the most complex and technologically important electrochemical reactions. High ORR overpotential is the source of major voltage losses in polymer electrolyte fuel cells [1]. Despite numerous efforts, the ORR mechanism has not been fully understood yet even for Pt electrodes, although these have been studied most extensively (see, e.g. review articles [2–6]). Hence, investigation of the ORR on various electrode materials continues attracting attention of experimentalists as well as of theoreticians.

In direct methanol fuel cells (DMFCs), methanol crossover through the polymer membrane from the anode to the cathode compartment with concomitant depolarization of the Pt cathode adds to the voltage losses decreasing efficiencies of DMFCs. Ruthenium-based cluster compounds containing selenium (Ru_xSe_y) have been introduced by Alonso Vante et al. [7–9] as methanol tolerant ORR catalysts. A method to prepare mixed non-stoichiometric Ru_xSe_y cluster materials has been suggested [9]. Later it has been found that the catalysts contained "Se-decorated" Ru particles rather than stoichiometric Ru_xSe_y compound [10–12]. Since then various procedures have been explored to prepare unsupported as well as carbon-supported Ru_xSe_y catalysts, which were investigated using electrochemical and structural methods [13–22]. However, despite numerous investigations, no consensus concerning the mechanism of the ORR on Ru_xSe_y catalysts and the role of Se in the enhancement of the catalytic activity has been reached yet.

In order to better understand the structure of Ru_xSe_y catalysts we have recently undertaken a systematic study of the structure evolution upon modification of carbon-supported Ru nanoparticles with the increasing amounts of Se [23]. Using a combination of TEM, XRD, XPS and EXAFS we have shown that deposition of Se on the surface of Ru nanoparticles results in formation of core-shell structures with hcp Ru core containing Ru selenide in their outer shell. Recently [24], the ORR kinetics on these catalyst samples was investigated using differential electrochemical mass spectrometry and double-disk electrode thin-layer flow-cell measurements. The authors have confirmed that modification of Ru/C catalyst with Se improves the ORR activity and reduces the tendency for H_2O_2 formation in the technically relevant potential region of 0.6–0.8 V vs. RHE.

The objective of this work is to better understand the role of Se in the ORR. We thus explore the kinetics of the ORR on Ru catalysts

* Corresponding author. Former address: Boreskov Institute of Catalysis, 630090 Novosibirsk, Russia. Tel.: +33 390 24 27 39; fax: +33 390 24 27 61.
E-mail address: Elena.Savinova@ecpm.u-strasbg.fr (E.R. Savinova).
[1] Present address: Department of Chemical Engineering, University of Bath, Bath BA2 7AY, United Kingdom.
[2] Present address: Tata Chemicals Limited, Innovation Centre, H. No. 1/16, Anmol Pride, Baner Road, Pune 411045, India.

0920-5861/$ – see front matter © 2009 Elsevier B.V. All rights reserved.
doi:10.1016/j.cattod.2009.01.019

modified with different amounts of Se with RDE at different O_2 partial pressures, and complement this data with *in situ* EXAFS investigation of the catalysts at Ru K and Se K-edge under the reaction conditions.

2. Experimental

2.1. Catalysts preparation and characterization

Preparation of Vulcan XC-72 supported Ru nanoparticles modified with various amounts of Se and their structural characterization with high resolution transmission electron microscopy (HRTEM), EDX, XRD, XPS and EXAFS has been described in detail in Ref. [23] and will be mentioned in this paper in as much as necessary for further discussion. Se-modified Ru/C samples with Se:Ru ratio from 0 to 1 (Table 1), were prepared by reacting carbon-supported 20 wt.% Ru/Vulcan XC-72 nanoparticles with SeO_2 in THF–water (1:1, v/v) mixture followed by reduction in a H_2 flow at 200 °C. The particle size for pristine Ru nanoparticles as determined in Ref. [23] from the particle size distributions reconstructed from TEM images was $d_N = \sum_i N_i d_i / \sum_i N_i = 3.9$ nm (number-average) and $d_S = \sum_i N_i d_i^3 / \sum_i N_i d_i^2 = 5.0$ nm (surface-average). Structural studies have confirmed that when Se is allowed to react with Ru nanoparticles, the size of *hcp* Ru core decreases, and a shell comprising Ru selenide is formed on the surface. The mass-average size of Ru core determined with XRD is given in Table 1.

2.2. Electrochemical measurements

Electrolyte solutions were prepared from Milli-Q water (18 MΩ cm) and H_2SO_4 (Suprapure, Merck or suprapure, Russia). The oxygen reduction kinetics on carbon-supported Ru_xSe_y catalysts of different composition was studied using rotating disc electrode (RDE). Thin catalyst layers were prepared by pipetting from 10 to 20 μl of aqueous suspension containing 1.5 mg ml^{-1} of Ru_xSe_y/Vulcan and 0.15 mg ml^{-1} Nafion® on the face (0.20 cm^2 geometric area) of a glassy carbon (GC) rod (polished to a mirror finish and cleaned in the ultrasonic bath in ethanol, acetone and water) and drying under the Ar flow. Nafion® was added in order to better spread the catalyst on the GC support and improve the adhesion. The resulting films were mechanically stable, and showed reproducible cyclic voltammograms (CVs). After each experiment Ru_xSe_y/Vulcan was removed from the substrate by wiping the surface under a water flow. Electrochemical measurements were carried out in a three-electrode cell at 298 K in 0.1 M H_2SO_4 solution saturated with Ar/O_2 mixtures containing 1, 3, 10, 50 and 100% O_2. The counter electrode was Pt foil and the reference electrode—mercury sulfate electrode (MSE) Hg/Hg_2SO_4/0.1 M H_2SO_4 connected to the working electrode compartment via Luggin capillary. Potentials were controlled using Autolab PGSTAT30 potentiostat and are quoted vs. reversible hydrogen electrode RHE (E_{MSE} = 0.73 V vs. RHE).

Table 1
Sample description.

No.	Description	Se:Ru (atomic ratio)	Abbreviation	Average size of Ru core[a], nm
1	20 wt.%Ru	0	Ru/C	5.5
2	17.3 wt.% Ru + 13.5 wt.%Se	1.0	Ru_1Se_1/C	~3
3	18.3 wt.% Ru + 8.5 wt.% Se	0.59	$Ru_1Se_{0.59}$/C	3.5
4	19.7 wt.% Ru + 4.5 wt.% Se	0.30	$Ru_1Se_{0.3}$/C	4
5	19.6 wt.% Ru + 2.2 wt.% Se	0.146	$Ru_1Se_{0.15}$/C	4

[a] From Ref. [23] as measured by XRD.

2.3. EXAFS measurements and data processing

In situ EXAFS spectra at Se K and Ru K-edges were obtained at the EXAFS Station of the Siberian Synchrotron Radiation Center. The storage ring VEPP-3 with the electron beam energy of 2 GeV and the average stored current of 90 mA was used as the radiation source, and a channel cut Si(1 1 1) crystal as monochromator. EXAFS measurements were performed in two different three-electrode spectroelectrochemical cells filled with 0.1 M H_2SO_4 solution, the first adapted for transmission (Ru K-edge) using ionization chambers as detectors, the second for fluorescence (Se K-edge) mode. The working electrodes were prepared by spreading the suspension containing the catalyst powder and Nafion® in water:isopropanol (2:3) mixture on 190 μm thick Toray Paper. Isopropanol was added in order to improve spreading of the catalyst on the hydrophobic surface of the Toray Paper. The resulting catalytic layers contained ca. 2 mg/cm^2 of the catalyst with 10 wt.% of Nafion®. Pt was used as a counter and mercury sulfate as a reference electrode. Measurements were performed at room temperature first in Ar and then in oxygen atmosphere under potentiostatic conditions. In order to explore the influence of the electrode polarization on the catalyst structure the electrode potential was increased from 0.05 to 0.750 V RHE in a stepwise manner.

The EXAFS spectra were treated using the standard procedure [25,26] by "Viper" code [27,28]. The background was removed by extrapolating the pre-edge region onto the EXAFS region by Victoreen's polynomials. Three cubic splines were used to simulate the smooth part of the absorption coefficient. The inflection point of the edge of the X-ray absorption spectrum was used as the initial point ($k = 0$) of the EXAFS spectrum. The radial distribution function (RDF) was calculated from the EXAFS spectra in $k\chi(k)$ as the modulus of the Fourier transform in the wave number intervals 3.3–11.5 and 3.3–12.5 Å^{-1} for Se K and Ru K-edges, respectively. Curve fitting procedure with EXCURV92 [29] code was employed to determine the co-ordination distances R and the *apparent co-ordination numbers* CN in similar wave number intervals after preliminary Fourier filtering using known XRD data for the bulk compounds. In order to diminish the number of independent variables, the Debye-Waller factors for all samples under study were fixed at 0.005 Å^2. The choice of the Debye-Waller factor has proven to be a reasonable compromise and allowed minimizing distortion of the fitted spectra. The quality of fit indicator (*R*-factor) in all cases was much below 20%, which proved good quality of the fits and reliability of selected structural models [29]. In order to judge the quality of the fits, the model fits and the experimental data were compared both in *R*- and *k*-space. Fig. 1 allows the reader to judge the quality of the fits. The relative errors may be estimated as 10–20% in the co-ordination numbers and 1–2% in the distances [26,30].

3. Results and discussion

3.1. Polarization in inert atmosphere

3.1.1. Cyclic voltammetry

Fig. 2a shows CVs for 20%Ru/Vulcan XC-72 in 0.1 M H_2SO_4 acquired at two different upper electrode potentials. The anodic and the corresponding cathodic peaks can be observed in the potential interval from 0.03 to 0.15 V vs. RHE. At more positive potentials a shallow anodic peak emerges in the potential interval from 0.2 to 0.7 V with a cathodic counterpart around 0.3 V. Comparison of Fig. 2a–c reveals that modification of the surface of Ru nanoparticles with Se results in drastic changes in CVs (note different scales in Fig. 2a–c): (i) the double layer splitting shrinks indicating the decrease in the interfacial capacitance, (ii) the peaks

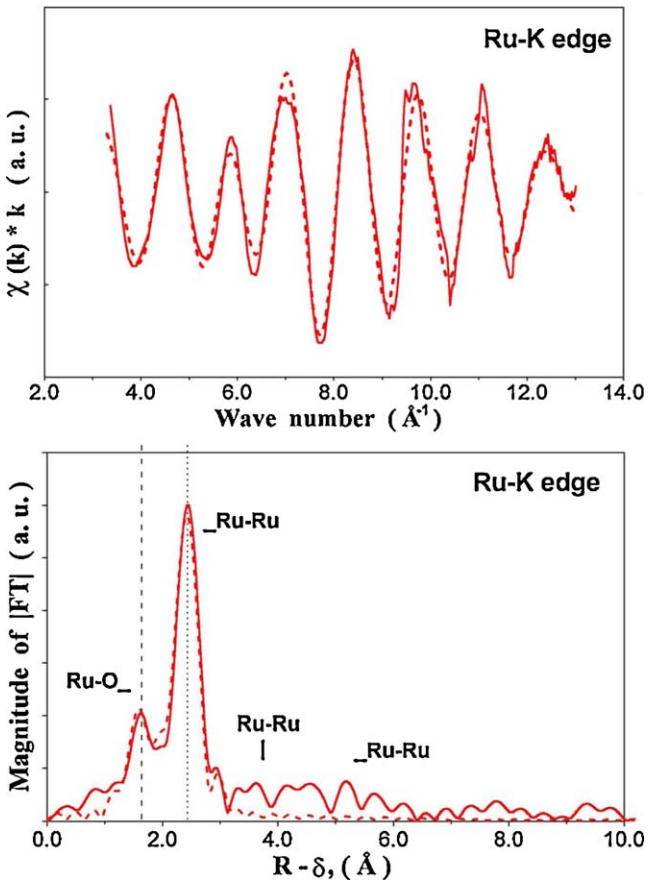

Fig. 1. The experimental data (solid) and model fits (dashed) in *k*- (upper panel) and *R*-space (lower panel) for Ru/C measured at Ru-edge in the electrochemical cell under O_2 atmosphere at 0.750 V vs. RHE.

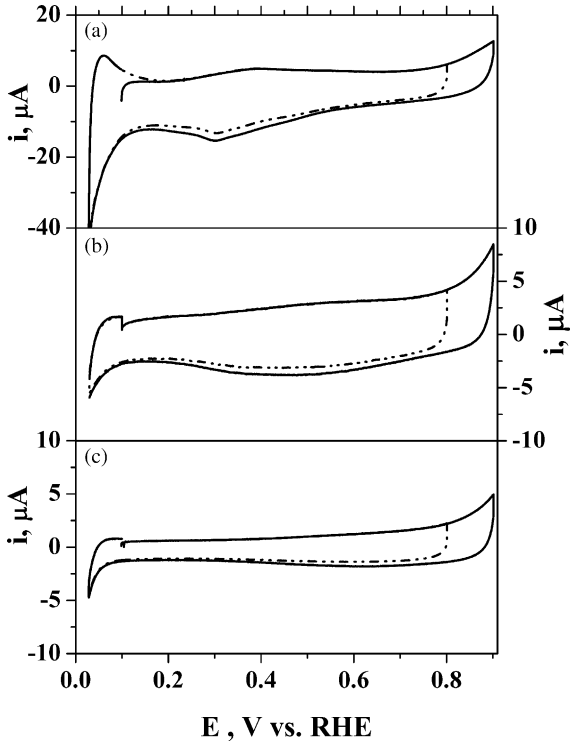

Fig. 2. CVs with two different anodic limits for Ru/C (a); $Ru_1Se_{0.3}$/C (b); and Ru_1Se_1/C (c) in 0.1 M H_2SO_4 at 298 K. Scan rate 5 mV s^{-1}. Catalysts (3×10^{-5} g) were deposited on glassy carbon support. Note different scales in the panels.

in the potential interval from 0.03 to 0.15 V disappear, and (iii) the anodic/cathodic peaks above 0.2 V decrease substantially and move to more positive potentials for Se/Ru = 0.3 and fully disappear for Se/Ru = 1.

3.1.2. *In situ* EXAFS

Ru/C and two Se-modified Ru/C samples (with Se:Ru = 1 and Se:Ru = 0.3) were studied using EXAFS in the electrochemical cell first under Ar, and then under O_2 atmosphere, in order to provide data concerning the interaction of the catalyst surface with water and oxygen, respectively. Fig. 3a represents the radial distribution functions obtained via Fourier transformation of the EXAFS spectra for Ru/C sample taken at Ru K-edge in the electrochemical cell under Ar atmosphere at different electrode potentials in the ORR potential range (solid lines), and for comparison also the RDFs measured *ex situ* under the ambient conditions (dotted line). All RDFs show a peak corresponding to Ru–Ru interactions in the first shell, the peaks at shorter distances due to Ru-O interactions and a few maxima at longer distances corresponding to Ru–Ru in the higher shells. Polarization at 0.05 V strongly decreases the maximum corresponding to R-O bonds. In agreement with the earlier EXAFS studies [10,11], this suggests that under the ambient conditions Ru particles are covered with oxygen, and the latter is electrochemically desorbed upon polarization at 0.05 V. However, the fitting (see Table 2) suggests that even at 0.05 V oxygen neighbors are present in the co-ordination shell of Ru at R(Ru-O) = 2.06 Å. Shifting the electrode potential from 0.05 to 0.75 V, results in a small increase in the intensity corresponding to Ru-O bond at 2.06 Å and an emergence of a new maximum at shorter distances corresponding to Ru-O at 1.91 Å (Table 2). The latter coincides with the short (1.92 Å) distance in RuO_2 oxide [31].

When the surface of Ru particles is modified with Se (Figs. 4a and 5a), the differences between the samples stored in air and reduced in the electrochemical cell are diminished, and for Ru_1Se_1/C become negligible. Also negligible are the changes induced in the catalyst structure by the anodic polarization. It should be noted that in order that the fitting quality were satisfactory, oxygen was introduced in the first co-ordination shell of Ru (Tables 3 and 4). However, the Ru-O CNs are independent of the electrode potential, and decrease with the increase in Se content. The latter suggests that Ru-O distances for Se-containing samples either correspond to non-dissociative water adsorption, or are artifacts arising from fixing Debye-Waller factors and from neglecting Se neighbors for $Ru_1Se_{0.3}$/C.

Figs. 6 and 7 show RDFs obtained via Fourier transformation of the *in situ* Se K-edge EXAFS spectra for $Ru_1Se_{0.3}$/C and Ru_1Se_1/C samples, respectively. The RDFs measured *ex situ* under the ambient conditions are shown as dotted lines for comparison. The main peak due to Se–Ru and Se–Se interactions is observed at R–δ = 2.3 Å. A side peak at shorter distances arises due the Ramsauer-Townsend resonance (see Ref. [32]) and partially overlaps with the peak due to Se-O interactions. Comparison of the RDFs for the samples measured *ex situ* and those after polarization at 0.05 V RHE suggests that Se, which is partially oxidized upon storage in ambient atmosphere [23], is reduced in the electrochemical cell. This is in agreement with the recent study of Inukai et al. [32]. The oxidation under ambient conditions is more pronounced for the sample containing larger amount of Se (*cf.* dotted curves in Figs. 6 and 7).

The co-ordination distances and the apparent co-ordination numbers obtained from fitting of the spectra for $Ru_1Se_{0.3}$/C sample are represented in Table 5. The Se-Ru distance of 2.52 Å is somewhat larger than that obtained from fitting Ru K-edge EXAFS

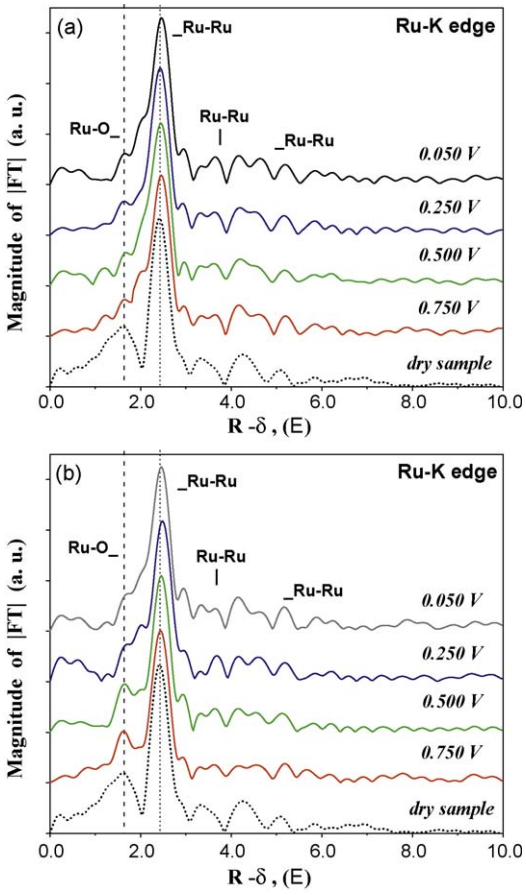

Fig. 3. Radial distribution functions for Ru/C obtained via Fourier transformation of k^1-weighted $\chi(k)$ measured at Ru-edge in the electrochemical cell under Ar (a) and O_2 (b) atmosphere at different electrode potentials: 0.050 V (black), 0.250 V (blue), 0.500 V (green) and 0.750 V vs. RHE (red). RDF for dry sample under ambient conditions is shown as a dotted line. Distance ($R-\delta_i$) is given in Å. (For interpretation of the references to color in this figure legend, the reader is referred to the web version of the article.)

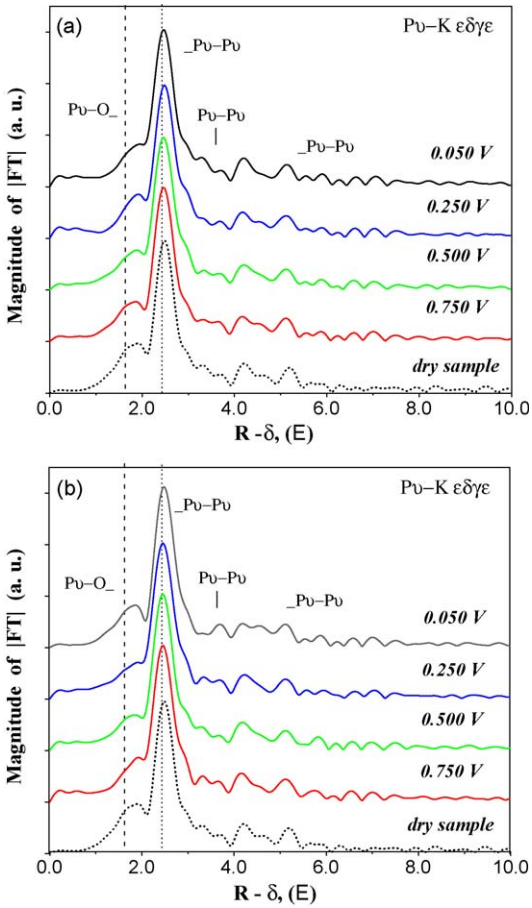

Fig. 4. Radial distribution functions for $Ru_1Se_{0.3}$/C obtained via Fourier transformation of k^1-weighted $\chi(k)$ measured at Ru-edge in the electrochemical cell under Ar (a) and O_2 (b) atmosphere at different electrode potentials: For line colors see Fig. 3. (For interpretation of the references to color in this figure legend, the reader is referred to the web version of the article.)

spectra, but the difference is within the characteristic accuracy of EXAFS. The apparent CNs for Se-Ru and Se-Se (at 2.48 Å) are equal to 2.0 ± 0.1 and 0.9 ± 0.1, correspondingly, and in agreement with the results of Inukai et al. [32]. In order to obtain a satisfactory fit, oxygen neighbors were introduced in the co-ordination shell at 1.55 ± 0.02 and 1.76 ± 0.01 Å for the samples both in Ar and in O_2. However, contrary to what has been reported by Inukai et al. [32], we did not observe significant changes in the Se-O CNs with the electrode potential. We thus tentatively attribute oxygen in the co-ordination shell of Se to chemisorbed water. Anodic polarization of the electrode up to 0.75 V RHE does not lead to any alteration of the RDFs in Ar atmosphere, confirming the stability of Ru_xSe_y catalysts in the potential interval from 0.05 to 0.75 V vs. RHE.

3.1.3. Interfacial properties of unmodified and Se-modified Ru particles

The *in situ* EXAFS data suggest that the surface of pristine carbon-supported Ru particles is covered with some oxygen-containing species in the whole potential interval explored, and their surface coverage increases with the potential shift from 0.03 to 0.75 V vs. RHE. To quantify the oxygen coverage on Ru, the CV of Ru/C was integrated and the charge obtained was corrected for the carbon support contribution and double layer charging. The charge in the interval from 0.03 to 0.8 V was equal to 0.960 mC/cm^2, while that between 0.2 to 0.8 V to 0.750 mC/cm^2. The latter corresponds to transfer of ca. 3e$^-$ per surface Ru atom.

Table 2
Distances (R) and co-ordination numbers (CN) for Ru/C sample calculated from Ru K-edge EXAFS spectra measured under ambient conditions (a) and in spectroelectrochemical cell under argon (b) and oxygen (c) atmosphere[a].

Ru/C	Dry sample (a)		*In situ* under argon (b)								*In situ* under oxygen (c)							
Shell	R, Å	CN	0.050 V		0.250 V		0.500 V		0.750 V		0.050 V		0.250 V		0.500 V		0.750 V	
			R, Å	CN	R, Å	CN	R, Å	CN	R, Å	CN	R, Å	CN	R, Å	CN	R, Å	CN	R, Å	CN
Ru-O	1.92	0.9	1.90	0.1	1.90	0.2	1.91	0.4	1.91	0.5	1.91	0.1	1.92	0.1	1.90	0.1	1.91	0.5
Ru-O	2.05	1.6	2.06	0.5	2.06	0.6	2.07	0.5	2.06	0.7	2.07	0.7	2.07	0.7	2.05	1.2	2.05	1.3
Ru–Ru	2.63	4.8	2.63	4.7	2.63	4.7	2.63	4.6	2.63	4.6	2.63	4.7	2.63	4.6	2.63	4.4	2.62	4.2
Ru–Ru	2.73	5.1	2.73	5.1	2.73	5.1	2.73	5.1	2.73	5.0	2.73	5.0	2.73	5.0	2.72	5.0	2.73	5.0

[a] The values of Debye-Waller factors are fixed at 0.005 Å^2.

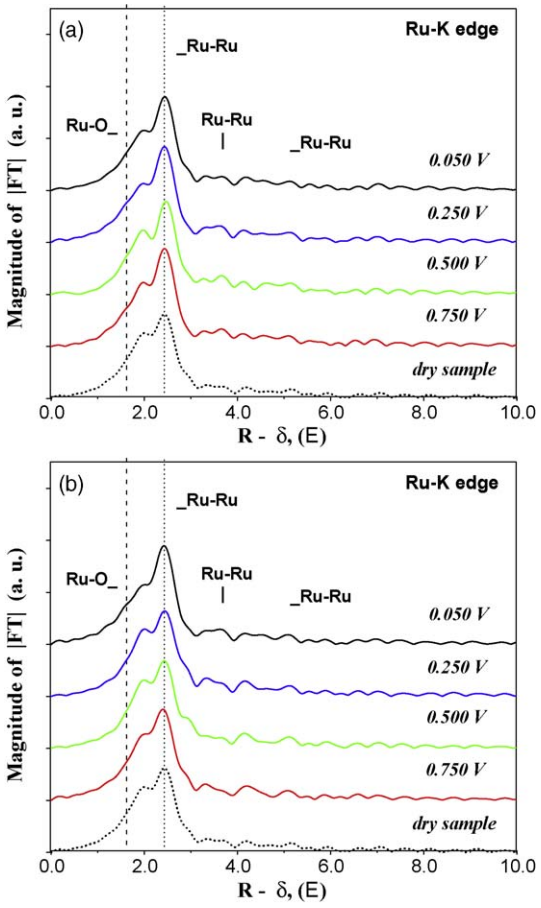

Fig. 5. Radial distribution functions for Ru_1Se_1/C obtained via Fourier transformation of k^1-weighted $\chi(k)$ measured at Ru-edge in the electrochemical cell under Ar (a) and O_2 (b) atmosphere at different electrode potentials. For line colors see Fig. 3. (For interpretation of the references to color in this figure legend, the reader is referred to the web version of the article.)

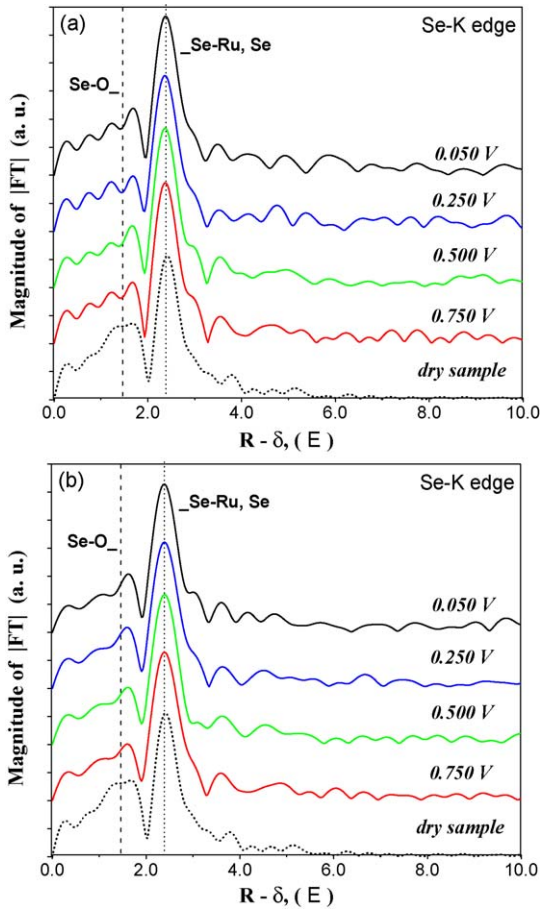

Fig. 6. Radial distribution functions for $Ru_1Se_{0.3}/C$ obtained via Fourier transformation of k^1-weighted $\chi(k)$ measured at Se K-edge in the electrochemical cell under Ar (a) and O_2 (b) atmosphere at different electrode potentials. For line colors see Fig. 3. (For interpretation of the references to color in this figure legend, the reader is referred to the web version of the article.)

Table 3
Distances (R) and co-ordination numbers (CN) for $Ru_1Se_{0.3}/C$ sample calculated from Ru K-edge EXAFS spectra measured under ambient conditions (a) and in spectroelectrochemical cell under argon (b) and oxygen (c) atmosphere[a].

$Ru_1Se0.3/C$	Dry sample (a)		*In situ* under argon (b)								*In situ* under oxygen (c)							
Shell	R, Å	CN	0.050 V		0.250 V		0.050 V		0.750 V		0.050 V		0.250 V		0.500 V		0.750 V	
			R, Å	CN	R, Å	CN	R, Å	CN	R, Å	CN	R, Å	CN	R, Å	CN	R, Å	CN	R, Å	CN
Ru-O	1.93	0.5	1.92	0.3	1.92	0.2	1.93	0.4	1.93	0.4	1.92	0.4	1.92	0.4	1.92	0.4	1.92	0.4
Ru-O	2.06	0.8	2.07	0.7	2.07	0.7	2.07	0.7	2.07	0.7	2.07	0.7	2.07	0.6	2.07	0.6	2.08	0.7
Ru–Ru	2.62	4.0	2.63	4.2	2.62	4.0	2.62	4.0	2.61	4.0	2.63	4.2	2.62	4.1	2.63	4.1	2.63	4.1
Ru–Ru	2.73	5.0	2.73	5.0	2.73	5.0	2.73	5.0	2.72	5.0	2.73	5.1	2.73	5.1	2.72	5.1	2.73	5.1

[a] The values of Debye-Waller factors are fixed at 0.005 $Å^2$.

Table 4
Distances (R) and co-ordination numbers (CN) for Ru_1Se_1/C sample calculated from Ru K-edge EXAFS spectra measured under ambient conditions (a) and in spectroelectrochemical cell under argon (b) and oxygen (c) atmosphere[a].

Ru1Se1/C	Dry sample (a)		*In situ* under argon (b)								*In situ* under oxygen (c)							
Shell	R, Å	CN	0.050 V		0.250 V		0.500 V		0.750 V		0.050 V		0.250 V		0.500 V		0.750 V	
			R, Å	CN	R, Å	CN	R, Å	CN	R, Å	CN	R, Å	CN	R, Å	CN	R, Å	CN	R, Å	CN
Ru-O	1.95	0.4	1.97	0.5	1.97	0.5	1.96	0.5	1.95	0.5	1.96	0.5	1.95	0.4	1.96	0.3	1.95	0.4
Ru-Se	2.44	1.2	2.44	1.1	2.44	1.1	2.44	1.2	2.45	1.2	2.43	1.1	2.44	1.3	2.45	1.3	2.45	1.3
Ru–Ru	2.64	2.5	2.64	2.7	2.64	2.7	2.64	2.7	2.64	2.7	2.64	2.7	2.63	2.6	2.64	2.6	2.63	2.6
Ru–Ru	2.74	2.8	2.73	2.8	2.73	2.9	2.74	2.8	2.74	2.9	2.73	2.9	2.74	2.8	2.73	2.9	2.73	2.9
Ru–Ru	3.10	0.0	3.10	0.0	3.10	0.0	3.10	0.0	3.10	0.0	3.10	0.0	3.10	0.0	3.10	0.0	3.10	0.0

[a] The values of Debye-Waller factors are fixed at 0.005 $Å^2$.

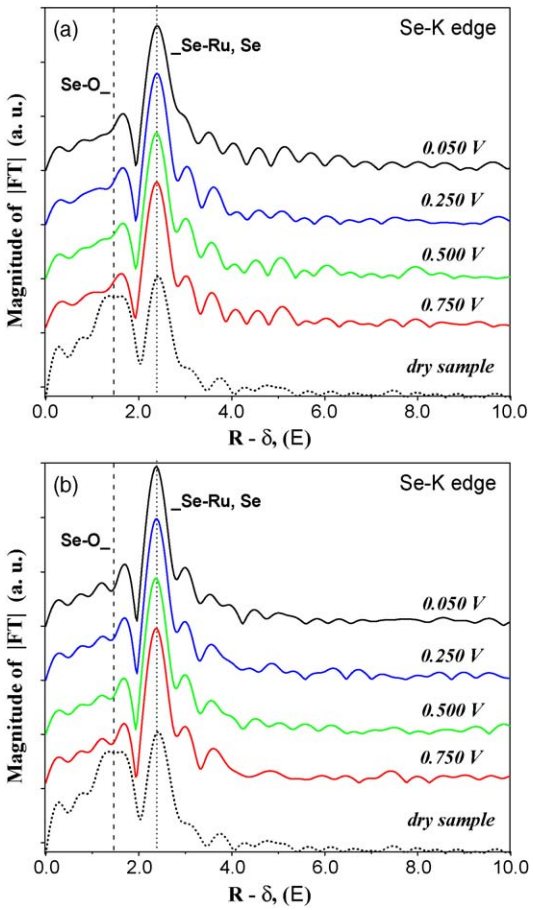

Fig. 7. Radial distribution functions for Ru_1Se_1/C obtained via Fourier transformation of k^1-weighted $\chi(k)$ measured at Se K-edge in the electrochemical cell under Ar (a) and O_2 (b) atmosphere at different electrode potentials. For line colors see Fig. 3. (For interpretation of the references to color in this figure legend, the reader is referred to the web version of the article.)

In order to better understand the origin of the oxygen species, we turn to the literature data. Investigations of the interfacial properties of Ru electrodes date back to the works of Entina and Petrii [33], who showed that the potential of zero total charge (pztc) for electrodeposited Ru lies below zero on the RHE scale, and that the potential intervals of H and OH adsorption cannot be fully separated. The electrochemical properties of Ru single crystals were studied in a number of more recent publications [34–38]. Based on the CO displacement measurements, voltammetric peaks for Ru(0 0 0 1) in the interval from 0.03 to 0.15 V were attributed to the OH_{ads} formation/reduction [39]. The oxidation of more open Ru $(1\,0\,\bar{1}\,0)$ is substantially more facile, and evidences a high structural sensitivity of the surface oxidation [38]. Voltammetric features above 0.2 V were ascribed to the build-up of an oxygen adlayer originating from water splitting [34,35,38]. Lin et al. [34], using *ex situ* LEED, identified a variety of adlayer structures on the emersed Ru(0 0 0 1) electrodes with the increasing electrode potential: from (2×2)-O via (3×1)-O to (1×1)-O. According to El-Aziz and Kibler [39], the maximum OH_{ads} coverage on Ru(0 0 0 1) in $HClO_4$ is 0.4 ML, while the oxygen coverage reaches 1 ML at 0.8 V vs. saturated calomel electrode (SCE).

The *in situ* EXAFS data of this work corroborate the attribution of the voltammetric peaks (see Refs. [38,39]) in the interval from 0.0 to 0.15 V vs. RHE to the electrochemical adsorption/desorption of some oxygen-containing species, most likely OH_{ads}. The Ru-O bond distances detected in this work are consistent with the literature data. Indeed, Wang et al. [36] in their *in situ* X-ray reflectivity study of Ru(0 0 0 1) oxidation identified the bond distance of 2.04 Å with the adsorbed oxygen. In Ref. [40] the bond distances for oxygen-containing adsorbates on PtRu alloy were determined using the density functional theory (*dft*). For Ru-OH_{ads} and Ru-OH_{2ads} the Ru-O distances were calculated as 1.94 and 2.20 Å, respectively. As confirmed by the electrochemical and XAS data, above 0.15 V the surface oxidation persists, resulting in the increase of the surface coverage with the oxygen-containing species. Although the bond distances alone cannot provide an evidence of the nature of the adsorbates, it is likely that in agreement with the literature data, above 0.15 V, OH_{ads} is transformed into O_{ads} and ultimately a film of RuO_2 surface oxide. The charge (0.750 mC/cm^2) transferred in the potential interval from 0.2 to 0.8 V allows to estimate the oxygen coverage as ca. 1.5 ML. This is a reasonable value, considering 1 ML observed by El-Aziz and Kibler [39] for Ru(0 0 0 1), and assuming that Ru particles are more susceptible to oxidation compared to the close-packed surface. Such a high value suggests that oxygen atoms also penetrate in the subsurface layer, likely giving rise to a film of surface oxide.

Addition of Se leads to the suppression of OH_{ads} formation on Ru sites (*cf.* Fig. 2a–c), and inhibition of the surface oxide. This conclusion is in agreement with the earlier observations [8,11–13,23,24].

3.2. The oxygen reduction reaction

3.2.1. In situ EXAFS

The RDF curves for Ru/C, $Ru_1Se_{0.3}/C$ and Ru_1Se_1/C at various electrode potentials in the oxygen atmosphere are represented in Figs. 3b, 4b and 5b, respectively. We first concentrate on Ru/C, and compare Fig. 3a and b. In the presence of oxygen in the potential interval positive of 0.250 V the intensity of the peaks corresponding to Ru-O neighbors increases substantially compared to that in Ar. Fitting the EXAFS data suggests that positive polarization results in an increase in the number of Ru-O neighbors, and some decrease of Ru–Ru neighbors (Table 2). This is in agreement with what has previously been observed for Ru chalcogenide ORR

Table 5
Distances (R) and co-ordination numbers (CN) for $Ru_1Se_{0.3}/C$ sample calculated from Se K-edge EXAFS spectra *in situ* in the spectroelectrochemical cell under argon and oxygen atmosphere[a].

$Ru_1Se_{0.3}/C$	*In situ* under argon								*In situ* under Oxygen							
	0.050 V		0.250 V		0.500 V		0.750 V		0.050 V		0.250 V		0.500 V		0.750 V	
	R, Å	CN	R, Å	CN	R, Å	CN	R, Å	CN	R, Å	CN	R, Å	CN	R, Å	CN	R, Å	CN
Se-O	1.57	0.2	1.57	0.2	1.57	0.2	1.56	0.2	1.55	0.2	1.55	0.2	1.55	0.2	1.55	0.2
Se-O	1.77	0.5	1.77	0.4	1.76	0.4	1.77	0.4	1.76	0.4	1.77	0.5	1.76	0.4	1.76	0.4
Se-Se	2.48	0.9	2.48	0.9	2.47	1.0	2.47	1.0	2.48	0.9	2.47	0.9	2.48	0.9	2.48	0.9
Se-Ru	2.52	2.0	2.52	2.0	2.52	2.0	2.52	2.0	2.52	2.0	2.52	2.0	2.52	2.0	2.52	2.0
Se-Se	3.36	0.3	3.36	0.3	3.37	0.3	3.37	0.3	3.37	0.3	3.37	0.3	3.36	0.2	3.37	0.3

[a] The values of Debye-Waller factors are fixed at 0.005 Å^2.

catalysts [11], where it has also been demonstrated that potential reversal to 0.05 V allowed to re-establish low Ru-O CNs. Thus, the EXAFS data suggest that molecular oxygen interacts with the surface of Ru particles and leads to formation of a potential-dependent adlayer of oxygen-containing species. Since the values of CNs calculated from fitting the EXAFS spectra are apparent, they cannot be *directly* recalculated into coverages. However, taking into account that the cumulative CNs for Ru-O at 1.90 ± 0.02 and 2.05 ± 0.02 Å calculated from fitting EXAFS spectra (Table 2) in the presence of O_2 ca. 1.5 times exceed those observed in Ar, we infer that under the conditions of the ORR the overall surface coverage with oxygen species exceeds 2 ML. However, the nature of these adsorbates cannot be unambiguously ascertained from the EXAFS data alone. We thus turn to the literature data on the interaction of O_2 with Ru.

It has been established that interaction of O_2 with Ru(0 0 0 1) in UHV at room temperature results in formation of (2 × 2) adlayer of *atomic* oxygen with the coverage $\theta = 0.25$ [41,42] (see also review article [43] and refs. therein). An increase in the oxygen pressure to 1 bar leads to formation of (1 × 1)-O adlayer with $\theta = 1$ [44]. On Ru(0 0 0 1) the binding energy decreases, while Ru-O bond distance decreases from 2.03 ± 0.06 Å at $\theta = 0.25$ to 2.00 ± 0.04 Å at $\theta = 1.0$. At solid/liquid interface one must also consider possible influence of water and anions on the oxygen dissociative adsorption. Jacob and Goddard in their recent publication [45] using *dft* demonstrated that the activation barrier of O_2 dissociation on the surface of Pt does not change substantially in the presence of water. As to the influence of (bi)sulfate, we refer to the recent publication by Jin et al. [46], who using *in situ* FTIR spectroscopy documented that under positive polarization surface (hydro)oxide replaces bisulfate adsorbates on Ru(0 0 0 1) electrode. Although an unambiguous conclusion is not possible at this stage, considering the literature data, we tentatively attribute oxygen species observed with *in situ* EXAFS to the product(s) of *dissociative adsorption of* O_2: $O(H)_{ads}$ and/or surface (hydro)oxides.

The modification of Ru particles with Se inhibits their interaction with O_2: the higher the amount of Se, the smaller the changes observed in Fourier transforms of the EXAFS spectra at Ru K-edge in the O_2 atmosphere (Figs. 4b and 5b and Tables 3 and 4). No changes were observed in Fourier transforms of *in situ* Se K-edge spectra in the potential interval of the ORR. Note that Se is located on the surface of Ru particles, and thus the co-ordination shell of Se is much more sensitive to adsorption that the co-ordination shell of Ru. Thus the independence of R and CN of the electrode potential strongly suggests that Se is not directly involved in the catalytic act of the ORR on Se-modified Ru and supports earlier conclusion that oxygen adsorption and reaction occurs on Ru surface sites [11]. This conclusion is in agreement with the recent work of Inukai et al. [32].

3.2.2. The rotating disc studies

The oxygen reduction kinetics on carbon-supported Ru_xSe_y catalysts of different compositions was studied using RDE at different rotation rates ω ranging from 400 to 3600 rotations per minute (rpm). The reciprocal values of the experimental currents ($1/i$) were plotted vs. $\omega^{-0.5}$ for different electrode potentials (Koutecky-Levich plots, not shown) and proved to be linear in the potential interval investigated. The slopes obtained from the linearization of the experimental data within ± 10% agreed with the theoretical calculated using Levich equation [47]:

$$B = 0.620nFD_{O_2}^{2/3}\nu^{-1/6}C_{O_2}\omega^{1/2} \quad (1)$$

assuming that $n = 4$, and oxygen concentration C_{O_2}, viscosity ν and diffusion coefficient D_{O_2} in 0.1 M H_2SO_4 are the same as in pure water. Kinetic currents were extracted from the experimental data

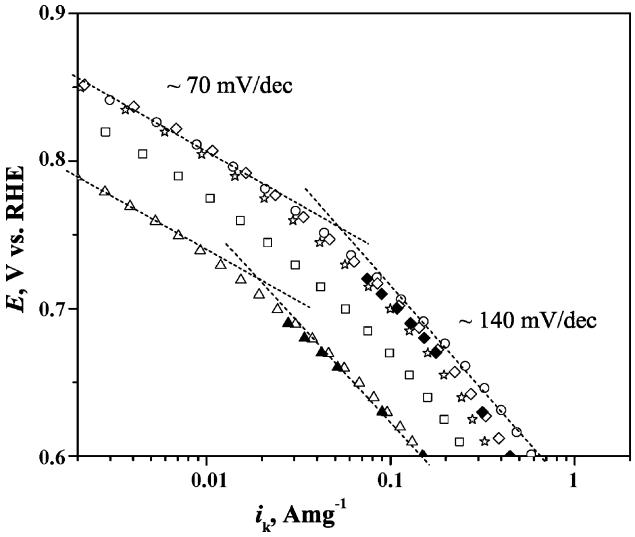

Fig. 8. Mass transport corrected currents calculated from the positive sweeps of RDE voltammograms acquired in 100% O_2-saturated 0.1 M H_2SO_4 electrolyte for Ru/C (triangles); $Ru_1Se_{0.15}$/C (circles); $Ru_1Se_{0.3}$/C (diamonds); $Ru_1Se_{0.59}$/C (stars) and Ru_1Se_1/C (squares). Measurements were performed at 298 K with the scan rate 1 mV s^{-1} and referred to 1 mg of Ru. Filled symbols stand for currents determined from the intercepts of Koutecky-Levich plots, open symbols correspond to the currents calculated using single RDE curves (see text for details).

using two different approaches: either (a) from the intercepts ($1/i_k$) of Koutecky-Levich plots, or, alternatively, (b) from selected RDE curves measured at a constant rotation rate using Eq. (2):

$$i_k = \frac{i \cdot i_d}{i_d - i} \quad (2)$$

Here i_d is the mass transport limited current. Since the exact nature of the active sites on Se-modified Ru has not been fully understood yet, in Fig. 8 we compare the values of the mass (referred to a mg of Ru) rather than specific activities for the samples containing different amounts of Se. As to the determination of the number of Ru surface sites on Ru_xSe_y catalysts, the reader is referred to the recent publications of Colmenares et al. [24] and Bogolowski et al. [20] In agreement with the literature data [8,13,23,24,48,49], Fig. 8 shows that the addition of Se to Ru considerably decreases the ORR overpotential. The dependence of the ORR activity on the Se/Ru ratio is demonstrated in Fig. 9, which shows a volcano-type behavior. It is evident that relatively small amounts of Se (Se/Ru = 0.15) are needed in order to achieve ca. 10 times increase in the ORR activity. Considering the size of Ru nanoparticles, the *apparent* Se coverage[3] can be estimated as ca. 0.5 monolayer for $Ru_1Se_{0.15}$/C sample. Further increase in Se loading results in a decrease of the ORR activity. However, even at high Se loadings the activity of the catalyst is still higher than for pure Ru.

Tafel slopes are often used as a criterion for the analysis of the mechanisms of electrochemical reactions. The experimental data obtained at different O_2 pressures demonstrate that Tafel slopes for Ru/C and Ru_xSe_y catalysts change continuously from ca. −140 mV/dec at 0.5 V to ca. −70 mV/dec at 0.8 V vs. RHE. It is noteworthy that similar Tafel slopes are observed for pristine Ru particles and those modified with different amounts of Se (Fig. 8).

The reaction orders in O_2 were determined for three samples: Ru/C; $Ru_1Se_{0.15}$/C and Ru_1Se_1/C. Fig. 10 represents a typical plot of $\lg(i_k)$ vs. $\lg(p_{O_2})$ for $Ru_1Se_{0.15}$/C sample. The reaction order is close to 1 in the potential interval from 0.5 to 0.75 V vs. RHE (1.04 ± 0.05, 0.97 ± 0.05 and 0.95 ± 0.05 for Ru/C; $Ru_1Se_{0.15}$/C and Ru_1Se_1/C respectively), and does not change substantially upon addition of Se.

[3] Assuming one Se per one surface Ru atom.

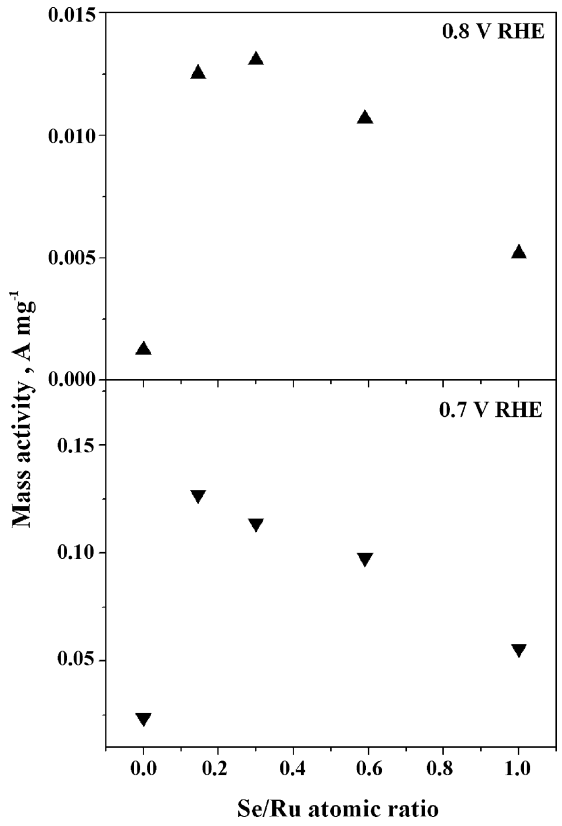

Fig. 9. The influence of Se/Ru ratio on the ORR transport corrected ORR currents (A/$mg_{(Ru)}$) at 0.8 V (a), and 0.7 V vs. RHE (b).

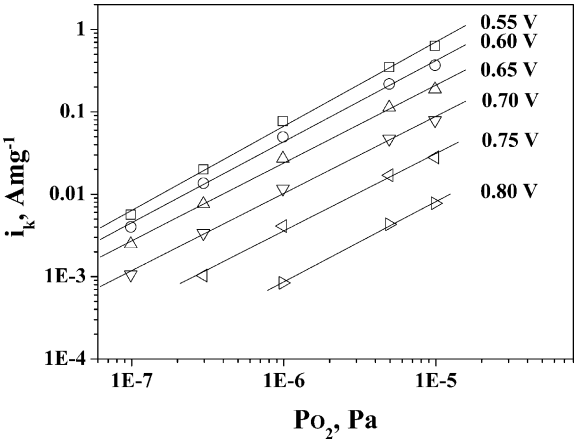

Fig. 10. Logarithmic plot of the mass transport corrected ORR currents (A/$mg_{(Ru)}$) for $Ru_1Se_{0.15}$/C sample vs. O_2 partial pressure. The pressure is given in Pa, the electrode potentials in V vs. RHE.

It is worth comparing the kinetic data for Ru/C and Ru_xSe_y/C with the literature data. The Tafel slopes for polycrystalline Pt and for supported Pt nanoparticles in acidic solutions have been found to change from ca. −120 mV/dec in the potential interval below ca. 0.8 V vs. RHE to ca. −60 mV/dec at higher electrode potentials. The change in the Tafel slope for Pt was attributed to the build-up of Pt oxides on the electrode surface above 0.8 V vs. RHE. For polycrystalline Pt the reaction order in oxygen is 1 in both potential intervals [50]. These results were interpreted in terms of the addition of the first electron (probably coupled with the proton addition) to the adsorbed oxygen molecule as the *rds*. ORR on polycrystalline Ru electrodes was first studied by Nekrasov and Khrusheva [51] and later in a series of publications by Anastasijevic et al. in acidic [52] and alkaline [53,54] and by Prakash and Joachin in alkaline electrolyte [55]. The extent of the surface oxidation has a considerable detrimental effect on the kinetics of the ORR [52–54,56]. Based on the rotating ring-disc electrode (RRDE) studies, it was suggested that ORR on polycrystalline Ru [52–54] as well as on Ru(0 0 0 1) and (1 0 1 0) single crystals [56] predominantly occurs via direct 4e pathway with the first electron transfer being the *rds*. It should be noted, however, that low concentrations of the hydrogen peroxide intermediate detected at the ring of an RRDE cannot serve as a proof for direct 4e ORR path. Indeed, recent studies by Chen and Kucernak [57] and Schneider et al. [58] have convincingly demonstrated that the amount of H_2O_2 detected on Pt electrodes [58] strongly increases, while the effective number of electrons n_{eff} involved in the electrochemical ORR [57] decreases from ca. 4 to 3.5 electrons under the conditions of the enhanced mass transport.

3.2.3. On the influence of Se on the ORR

In this section we try to rationalize the obtained experimental data and discuss the role of Se in the ORR. Firstly, considering that the Tafel slopes and the reaction orders in oxygen do not change in the presence of Se (RDE data), and that oxygen is not co-ordinated to Se during the ORR (EXAFS data), we infer that *Se modification does not alter the rds of the ORR on Ru*. Secondly, the experimental results suggest that the change of the Tafel slope with potential for Ru/C and Ru-Se/C cannot be explained by the build-up of surface oxides as previously proposed for Pt. Indeed, combined XAS and electrochemical evidence prove that addition of Se greatly decreases the surface concentration of oxygen-containing species. Thus, if indeed the change in the Tafel slope originated from the formation of the adlayer of oxygen-containing species, the shape of i_k vs. E would have changed dramatically upon Se addition. Meanwhile, we do not observe such a change (Fig. 8).

Thirdly, we discuss how to rationalize significantly different oxygen coverages on unmodified and Se-modified Ru with the same *rds*. The answer to this question is not obvious since high oxygen coverage on unmodified Ru particles implies that the rate constants of the reaction steps controlling the (electro)chemical desorption of oxygen adsorbates are lower than those controlling the formation of the oxygen adsorbates; and the other way around for Se-modified Ru. At present we cannot propose a definite answer to this puzzle. As a working *hypothesis* we propose that the products of dissociative oxygen adsorption are not the active intermediates in the ORR but rather blocking species, and that the ORR on unmodified as well as on Se-modified Ru particles occurs via so-called "associative mechanism" [59] with an intermediate peroxo-species formation. Indeed, compared to "dissociative mechanism" which requires at least 2 adjacent surface sites [60–62], the "associative mechanism" is less demanding, and is likely to proceed also on the oxygen-covered and on Se-covered surface. We further propose that Se hinders dissociative adsorption of oxygen on Ru due to the electronic interaction with the latter. Recently Babu et al. [63] presented combined XPS and NMR evidence of the charge transfer from Ru to Se. This finding is in agreement with the earlier surface science studies suggesting that adsorption of electronegative atoms, such as S, O, Cl on the surface of noble and transition metals leads to a notable increase in the metal work function (see monograph [64] and references therein). This work function change has been found to result in the inhibition of dissociative adsorption of oxygen, and reduction in the binding energy of atomic oxygen with the surface [65], which is revealed by significant reduction in the oxygen desorption temperature [66]. However, the results of this work suggest that the role of Se cannot be limited to the decrease of the $O(H)_{ads}$ coverage, but must also be connected with an acceleration of the

rds, presumably via an electronic influence of Se. Our hypothesis is in agreement with the recent finding of Bonakdarpour et al. [67] who reported that at ultra-low Se-Ru/C catalyst loading of 5 μg/cm^2 the fraction of H_2O_2 produced at the cathode exceeded 50%, while at 92 μg/cm^2 it was below 5%. The fact that at high catalyst loadings hydrogen peroxide is either not detected or detected in rather small quantities, may be explained by the high probability of H_2O_2 readsorption and further electrochemical reduction or chemical disproportionation. High activity of RuO_2 towards catalytic hydrogen peroxide decomposition has been described in a number of reference, in particular Refs. [68,69].

Another question is how to rationalize the first order in oxygen with the high oxygen coverage for unmodified Ru. Recently, Zhdanov and Kasemo [70], have demonstrated that with O–O lateral interactions, the model based on the associative mechanism is able to predict the first-order kinetics in a wide range of pressure even if the O coverage is appreciable.

4. Conclusions

Using *in situ* EXAFS at Ru K-edge it is shown that positive polarization leads to formation of oxygen-containing adsorbates on the surface of Ru particles. These adsorbates are formed through dissociative adsorption of water in the inert atmosphere, and through dissociative adsorption of molecular oxygen in the oxygen atmosphere, in the latter case the quantity of the adsorbates is substantially higher. The addition of selenium prevents formation of the oxygen adlayer both in argon and in oxygen. The *in situ* EXAFS data at Se-edge suggest that Se is not directly involved in the oxygen chemisorption and in the ORR. The kinetics of the ORR on unmodified and on Se-modified ruthenium catalysts is investigated. The dependence of the ORR activity on Se/Ru ratio shows volcano-type behavior with ca. 10 fold increase of the mass activity at $0.1 < Se/Ru < 0.3$. The reaction order in oxygen for all the samples under study is close to 1. The Tafel slopes are independent of Se content and for all the catalysts studied change from ca. −70 to −140 mV/dec when the electrode potential is decreased from 0.8 to 0.5 V. It is suggested that the change of the Tafel slope is not related to the build-up of the oxygen adlayer.

Acknowledgements

Financial support from the German Federal Ministry of Education and Research (BMBF) under O2Red Network project (Agreement 01 SF 0302), and from the ANR (in the framework of ANR-06-CEXC-004) is gratefully appreciated. E.R.S. is grateful to R. Adzic and Z. Jusys for providing the reprints of their publications.

References

[1] W. Vielstich, A. Lamm, H.A. Gasteiger (Eds.), Handbook of Fuel Cells. Fundamentals, Technology and Applications, Vol. 2: Electrocatalysis, John Wiley & Sons, Chichester, 2003.
[2] M.R. Tarasevich, A. Sadkowski, E. Yeager, in: B.E. Conway, J.O.M. Bockris, E. Yeager, S.U.M. Khan, R.E. White (Eds.), Comprehensive Treatise of Electrochemistry, Vol. 7, Plenum Press, New York, 1983, p. 301.
[3] Damjanovic, in: O.J. Murphy, S. Srinivasan, B.E. Conway (Eds.), Electrochemistry in Transition, Plenum Press, New York, 1992, p. 107.
[4] K. Kinoshita, Electrochemical Oxygen Technology, John Wiley & Sons, New York, 1992.
[5] R. Adzic, in: J. Lipkowski, P.N. Ross (Eds.), Electrocatalysis, Vol. 102, Wiley-VCH, New York, 1998, p. 197.
[6] G. Gattrell, B. MacDougall, in: W. Vielstich, A. Lamm, H.A. Gasteiger (Eds.), Handbook of Fuel Cells—Fundamentals, Technology, Applications, Vol. 2: Electrocatalysis, John Wiley & Sons, 2003, p. 444.
[7] N. Alonso-Vante, M. Giersig, H. Tributsch, Journal of the Electrochemical Society 138 (1991) 639.
[8] N. Alonso-Vante, in: W. Vielstich, A. Lamm, H.A. Gasteiger (Eds.), Handbook of Fuel Cells. Fundamentals, Technology and Applications, Vol. 2: Electrocatalysis, John Wiley & Sons, Chichester, 2003, p. 534.
[9] O. Solorza-Feria, K. Ellmer, M. Giersig, N. Alonso-Vante, Electrochimica Acta 39 (1994) 1647.
[10] N. Alonso-Vante, I.V. Malakhov, S.G. Nikitenko, E.R. Savinova, D.I. Kochubey, Electrochimica Acta 47 (2002) 3807.
[11] I.V. Malakhov, S.G. Nikitenko, E.R. Savinova, D.I. Kochubey, N. Alonso-Vante, Journal of Physical Chemistry B 106 (2002) 1670.
[12] F. Dassenoy, W. Vogel, N. Alonso-Vante, Journal of Physical Chemistry B 106 (2002) 12152.
[13] M. Bron, P. Bogdanoff, S. Fiechter, I. Dorbandt, M. Hilgendorff, H. Schulenburg, H. Tributsch, Journal of Electroanalytical Chemistry 500 (2001) 510.
[14] A.C. Boucher, V. Le Rhun, F. Hahn, N. Alonso-Vante, Journal of Electroanalytical Chemistry 554 (2003) 379.
[15] L. Colmenares, Z. Jusys, R.J. Behm, Journal of Physical Chemistry C 111 (2007) 1273.
[16] A. Lewera, J. Inukai, W.P. Zhou, D. Cao, H.T. Duong, N. Alonso-Vante, A. Wieckowski, Electrochimica Acta 52 (2007) 5759.
[17] A. Racz, P. Bele, C. Cremers, U. Stimming, Journal of Applied Electrochemistry 37 (2007) 1455.
[18] C. Christenn, G. Steinhilber, M. Schulze, K.A. Friedrich, Journal of Applied Electrochemistry 37 (2007) 1463.
[19] G. Zehl, P. Bogdanoff, I. Dorbandt, S. Fiechter, K. Wippermann, C. Hartnig, Journal of Applied Electrochemistry 37 (2007) 1475.
[20] N. Bogolowski, T. Nagel, B. Lanova, S. Ernst, H. Baltruschat, K.S. Nagabhushana, H. Boennemann, Journal of Applied Electrochemistry 37 (2007) 1485.
[21] W. Vogel, N. Alonso-Vante, Journal of Catalysis 232 (2005) 395.
[22] H. Schulenburg, M. Hilgendorff, I. Dorbandt, J. Radnik, P. Bogdanoff, S. Fiechter, M. Bron, H. Tributsch, Journal of Power Sources 155 (2006) 47.
[23] V.I. Zaikovsii, K.S. Nagabhushana, V.V. Kriventsov, K.N. Loponov, S.V. Cherepanova, R.I. Kvon, H. Boennemann, D.I. Kochubey, E.R. Savinova, Journal of Physical Chemistry B 110 (2006) 6881.
[24] L. Colmenares, Z. Jusys, R.J. Behm, Langmuir 22 (2006) 10437.
[25] D.I. Kochubey, EXAFS Spectroscopy of Catalysts, Nauka, Novosibirsk, 1992 (in Russian).
[26] D.C. Koningsberger, B.L. Mojet, G.E.V. Dorssena, D.E. Ramaker, Topics in Catalysis 10 (2000) 143.
[27] K.V. Klementiev, Journal of Physics D: Applied Physics 34 (2001) 209.
[28] K.V. Klementiev, code VIPER for Windows, freeware: www.desy.de/~klmn/viper.html.
[29] N. Binsted, J.V. Campbell, S.J. Gurman, P.C. Stephenson, SERC Daresbury Laboratory EXCURV92 program (1991).
[30] A.E. Russell, A. Rose, Chemical Reviews 104 (2004) 4613.
[31] I.D. ICSD Collection Code 23961, 1997.
[32] J. Inukai, D. Cao, A. Wieckowski, K.C. Chang, A. Menzel, V. Komanicky, H. You, Journal of Physical Chemistry C 111 (2007) 16889.
[33] V.S. Entina, O.A. Petrii, *Elektrokhimiya* (Russian Journal of Electrochemistry) 4 (1968) 457.
[34] W.F. Lin, P.A. Christensen, A. Hamnett, M.S. Zei, G. Ertl, Journal of Physical Chemistry B 104 (2000) 6642.
[35] M.S. Zei, G. Ertl, Physical Chemistry Chemical Physics 2 (2000) 3855.
[36] J.X. Wang, N.S. Marinkovic, H. Zajonz, B.M. Ocko, R.R. Adzic, Journal of Physical Chemistry B 105 (2001) 2809.
[37] N.S. Marinkovic, J.X. Wang, H. Zajonz, R.R. Adzic, Journal of Electroanalytical Chemistry 500 (2001) 388.
[38] S.R. Brankovic, J.X. Wang, Y. Zhu, R. Sabatini, J. McBreen, R.R. Adzic, Journal of Electroanalytical Chemistry 524 (2002) 231.
[39] A.M. El-Aziz, L.A. Kibler, Electrochemistry Communications 4 (2002) 866.
[40] S. Desai, M. Neurock, Electrochimica Acta 48 (2003) 3759.
[41] T.E. Madey, H.A. Engelhardt, D. Menzel, Surface Science 48 (1975) 304.
[42] P. He, K. Jacobi, Physical Review B 55 (1997) 4751.
[43] H. Over, Progress in Surface Science 58 (1998) 249.
[44] M. Rossler, P. Geng, J. Wintterlin, Review of Scientific Instruments 76 (2005) 023705.
[45] T. Jacob, W.A. Goddard III, ChemPhysChem 7 (2006) 992.
[46] J.M. Jin, W.F. Lin, P.A. Christensen, Physical Chemistry Chemical Physics 10 (2008) 3774.
[47] A.J. Bard, L.R. Faulkner, Electrochemical Methods. Fundamentals and Applications, J. Wiley & Sons, NY, 2001.
[48] D. Cao, A. Wieckowski, J. Inukai, N. Alonso-Vante, Journal of the Electrochemical Society 153 (2006) A869.
[49] N. Alonso-Vante, H. Tributsch, O. Solorza-Feria, Electrochimica Acta 40 (1995) 567.
[50] A. Damjanovic, V. Brusic, Electrochimica Acta 12 (1967) 615.
[51] L.N. Nekrasov, E.I. Khrusheva, *Elektrokhimiya* (Russian Journal of Electrochemistry) 3 (1967) 166.
[52] N.A. Anastasijevic, Z.M. Dimitrijevic, R.R. Adzic, Electrochimica Acta 31 (1986) 1125.
[53] N.A. Anastasijevic, Z.M. Dimitrijevic, R.R. Adzic, Journal of Electroanalytical Chemistry 199 (1986) 351.
[54] N. Anastasijevic, Z.M. Dimitrijevic, R.R. Adzic, Electrochimica Acta 37 (1992) 457.
[55] J. Prakash, H. Joachin, Electrochimica Acta 45 (2000) 2289.
[56] H. Inoue, S.R. Brankovic, J.X. Wang, R.R. Adzic, Electrochimica Acta 47 (2002) 3777.
[57] S.L. Chen, A. Kucernak, Journal of Physical Chemistry B 108 (2004) 3262.
[58] A. Schneider, L. Colmenares, Y.E. Seidel, Z. Jusys, B. Wickman, B. Kasemo, R.J. Behm, Physical Chemistry Chemical Physics 10 (2008) 1931.
[59] J.K. Nørskov, J. Rossmeisl, A. Logadottir, L. Lindqvist, J.R. Kitchin, T. Bligaard, H. Jonsson, Journal of Physical Chemistry B 108 (2004) 17886.

[60] E. Yeager, Journal of Molecular Catalysis 38 (1986) 5.
[61] R.R. Adzic, J.X. Wang, Journal of Physical Chemistry B 102 (1998) 8988.
[62] R.A. Sidik, A.B. Anderson, Journal of Electroanalytical Chemistry 528 (2002) 69.
[63] P.K. Babu, A. Lewera, J.H. Chung, R. Hunger, W. Jaegermann, N. Alonso-Vante, A. Wieckowski, E. Oldfield, Journal of the American Chemical Society 129 (2007) 15140.
[64] Costas G. Vayenas, Symeon Bebelis, Costas Pliangos, Susanne Brosda, D. Tsiplakidis, Electrochemical Activation of Catalysis, Kluwer Academic/Plenum Publishers, New York, 2001.
[65] C.T. Campbell, M.T. Paffett, Applications of Surface Science 19 (1984) 28.
[66] R. Schennach, E. Bechtold, Surface Science 369 (1996) 277.
[67] A. Bonakdarpour, C. Delacote, R. Yang, A. Wieckowski, J.R. Dahn, Electrochemistry Communications 10 (2008) 611.
[68] R. Venkatachalapathy, G.P. Davila, J. Prakash, Electrochemistry Communications 1 (1999) 614.
[69] S.J. Updike, M.C. Shults, J.K. Kosovich, I. Treichel, P.M. Treichel, Analytical Chemistry 47 (1975) 1457.
[70] V.P. Zhdanov, B. Kasemo, Electrochemistry Communications 8 (2006) 1132.